Shape phase transition at $N = 88$–90 in ^{144,146}Ba

J. B. Gupta[1,*] and Mansi Saxena[2,3]
[1]*Ramjas College, University of Delhi, Delhi-110007, India*
[2]*Department of Physics & Astrophysics, University of Delhi, Delhi-110007, India*
[3]*Hindu College, University of Delhi, Delhi-110007, India*
(Received 11 January 2015; revised manuscript received 12 April 2015; published 12 May 2015)

Background: The neutron-rich Ba isotopes with only six valence protons represent the beginning of the collective rotation-vibration band structure. The sharp shape phase transition at $N = 88$–90 observed in Ce-Gd isotones is not exhibited in $^{144-146}$Ba, which renders their analysis interesting. Also there are ambiguities in the spin and band assignments.
Purpose: To study their spectra empirically and to compare with predictions from an interacting boson model and microscopic dynamic pairing plus quadrupole model to explain the smooth shape transition at $N = 88$–90.
Method: We compare the results of the calculation in the interacting boson models (IBM-1) and IBM-2 and the dynamic pairing plus quadrupole model with experiment and illustrate the variation in level structure of the Ba isotopes with N. The absence of sharp phase transition at $N = 88$–90 is examined.
Results: The ambiguous spin and parity of levels of the vibrational bands are assigned on the basis of calculated K components and the decay characteristics.
Conclusion: The second $I^\pi = 2^+$ states in ^{144,146}Ba have $K = 0$ predominance, and $I^\pi = 2_3^+$ states are $K = 2$. The smooth transition at $N = 88$–90 is explained.

DOI: 10.1103/PhysRevC.91.054312 PACS number(s): 21.60.Ev, 21.60.Fw, 21.10.Re, 27.60.+j

I. INTRODUCTION

The shape phase transition at $N = 88$–90 isotones of Nd-Dy has been known for a long time [1]. The important role of the $Z = 64$ subshell at $N \leqslant 88$ and its disappearance at $N = 90$, causing the maximum shape phase transition at Sm-Gd is also well recognized [2,3]. But, the occurrence of a maximum deformation in ^{144}Ba at $N = 88$ as compared to $Z > 56$ isotones of ^{146}Ce, ^{148}Nd, ^{150}Sm, and ^{152}Gd and a minimum change in ^{146}Ba, yielding a minimum deformation in the $N = 90$ isotones, is not well studied so far. With $E(2_1^+) =$ 199 keV in ^{144}Ba and 181 keV in ^{146}Ba [4], a difference of only 18 keV at $N = 88$–90 represents almost *no shape phase transition* in these Ba isotopes (Fig. 1). The energy ratios $R_{4/2}$ are 2.65 for ^{144}Ba and 2.84 for ^{146}Ba. Both are below the shape phase-transition value of $R_{4/2} = 3.0$ as defined by the $X(5)$ analytical symmetry [5], which is achieved in ^{148}Ba ($R_{4/2} =$ 2.984). Thus the degree of phase transition at $N = 88$–90 is a function of the atomic number Z too. The isotopes of ^{144,146}Ba are the most neutron-rich ones in which, besides the yrast band on the ground state, the vibrational bands of $K^\pi = 0_2^+$ and $K^\pi = 2^+$ are known [4]. In ^{148}Ba besides the ground-state band, only a 2_2^+ state is known. However, there is an ambiguity in the K-band assignment of $I^\pi = 2^+$ vibrational states in ^{144,146}Ba [4,6,7] as illustrated below.

In ^{144}Ba, the 1315-keV $I = 2_2$ state is listed as $(I = 2)$ (parity ambiguous) in Ref. [4], as 2_γ in Sakai's tables of 1984 [7], and the 1848-keV level is listed as 2_β. With a low-lying state 0_2^+ at 1020 keV, this is not probable. Another $I^\pi = 2^+$ state at 1864 keV is listed in Ref. [4]. It would be interesting to compare their decay character and possibly assign the two states to the $K = 0$ and 2 vibrational bands.

The energy-level spectrum of ^{146}Ba is not much different from the lighter $N = 88$ isotope ^{144}Ba, unlike the heavier Z isotones of Ce and (Nd-Dy) [4]. Here, we plan to study this phenomenon in more detail. Earlier, Scott *et al.* [8] studied ^{144,146}Ba in a $\gamma\gamma(\theta)$ angular correlation experiment and in the interacting boson model (IBM-1). A comparison with their work is also performed here. The spin-parity assignment of the 1115- and 1256-keV levels in ^{146}Ba are listed as $(1,2)^+$ in Ref. [4]. Higher up, a 1566-keV 2^+ level is included in Ref. [4]. Here we attempt to study the K assignment of these states. In Sec. II, the empirical data in this region are studied. Earlier, Kumar and Gupta [9] used the microscopic dynamic pairing plus quadrupole (DPPQ) model [10] for a detailed study of the light ($N < 82$) Ba isotopes. In Sec. III, a brief description of the Interacting boson models (model 1 and model 2) and the DPPQ model is given. In Sec. IV, results from the dynamic pairing plus quadrupole model (DPPQM) [10] are analyzed. The interacting boson model [11] IBM-1 provides an alternative method and has proved quite successful for the study of collective spectra [11]. The same is used for ^{144,146}Ba to compare with experiment. We also employ IBM-2 for further elucidation of their structure. In Sec. V, a summary and a discussion are given.

II. EMPIRICAL DATA ANALYSIS

A. Energy-level band structures

The energy levels in the rotational bands on the ground state in ^{144,146}Ba are extended up to $I^\pi = 16^+$. In Fig. 2, the energy ratios [4] $R_{I/2}(=E_I/E_2)$ are plotted versus the spin I for the ground-state bands. Note the almost *equal values* in the two spectra up to $I^\pi = 16^+$, indicating their similar static deformation characteristics. For the shape transitional nuclei,

*jbgupta2011@gmail.com

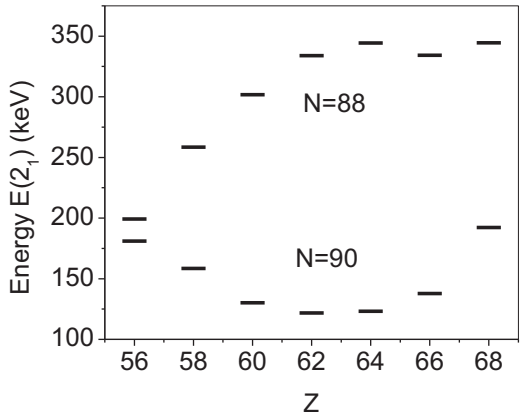

FIG. 1. Level energy $E(2_1^+)$ [4] in the ground band of Ba-Er for $N = 88$ and 90 isotones. Maximum rise and fall are at $Z = 64$ Gd. At $Z = 56$, the change is minimum.

if the rotation-vibration interaction term in Eq. (1) is ignored,

$$E(I) = aI(I+1) + bI + cI^2(I+1), \tag{1}$$

one obtains the linearity relation (2) for the energy ratios $R_{I/2}(=E_I/E_2)$ versus $R_{4/2}$ for the ground-state band [12],

$$R_{I/2} = R_{4/2}[I(I-2)/8] - I(I-4)/4. \tag{2}$$

The linear relation for ^{146}Ba (inverted triangles) is plotted in Fig. 2. The small deviations of $R_{I/2}$ from the linearity relation (2) are a measure of the rotation-vibration interaction in ^{144,146}Ba, which increases with spin, indicating the effects of rotation-vibration interaction and of the centrifugal stretching.

The partial energy spectra of ^{144,146}Ba are illustrated in Fig. 3. Although the ground bands are similar, and the 0_2^+ band head energy are also almost equal, the vibrational band structures are much different. In ^{144}Ba, $\Delta E_\beta = E(2_2) - E(0_2) = 295$ keV is larger than $E(2_1^+) = 199$ keV, and the higher two $I^\pi = 2^+$ states lie very close. In terms of the spherical vibration, the triplet of states (4_1^+, 0_2^+, and 2_2^+) do not form a split triplet here corresponding to an anharmonic vibrator. Instead, there is a tendency to form a K-band structure.

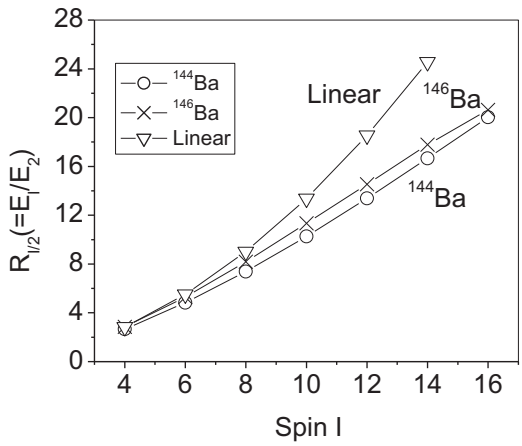

FIG. 2. The energy ratio [4] $R_{I/2}(=E_I/E_2)$ versus spin I in the ground-state bands of ^{144,146}Ba. The linear curve [Eq. (2)] is for ^{146}Ba.

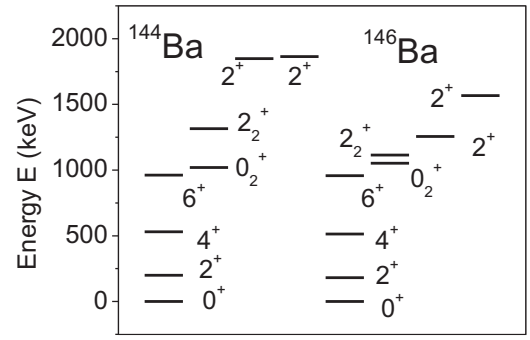

FIG. 3. The partial energy-level spectra [4] of ^{144,146}Ba.

In ^{146}Ba, the 1115-keV $I^\pi = (1,2)^+$ state is quite close to the 0_2^+ state and the other two $I^\pi = 2^+$ (1256-keV spin ambiguous and 1566-keV 2^+) states lie apart and much higher. No higher spin states are known [4]. In view of our analysis as given below, we have assigned the 1115- and 1256-keV states to $I^\pi = 2^+$ in Fig. 3.

In Fig. 4 we compare the spectrum of ^{144}Ba with one of $N = 88$ isotone ^{146}Ce. In Ce, with the addition of two protons, the collective bands are much better developed up to $I^\pi \leqslant 4^+$, although the energy spacing in the ground-state band is increased (more vibrational with smaller $R_{4/2} = 2.49$). This increased spacing with increasing Z is usually explained on the basis of a $Z = 64$ subshell effect [2,3]. In this case, the subshell effects reduce the proton boson number in ^{146}Ce from $N_p = 4$ to $N_p = 3$. But ^{144}Ba also has $N_p = 3$, so the picture is not so simple in terms of the dependence only on the boson numbers. Both protons and neutrons are important here as available in IBM-2. One has to go into greater detail (see below).

Microscopically, in Ba six protons occupy the down sloping Nilsson single-particle orbits. At $N = 88$, only six neutrons occupy the $\nu f_{7/2}$ and $\nu h_{9/2}$ orbits, and at $N = 90$ two more neutrons occupy these orbits. One needs to explain why the deformation is *maximum at* $N = 88$ *and minimum at* $N = 90$ in Ba as compared to higher Z isotones. A detailed explanation is given below.

We have used the phenomenological interacting boson models [11] IBM-1 and IBM-2 for a comparison. We also employ the microscopic dynamic pairing plus quadrupole

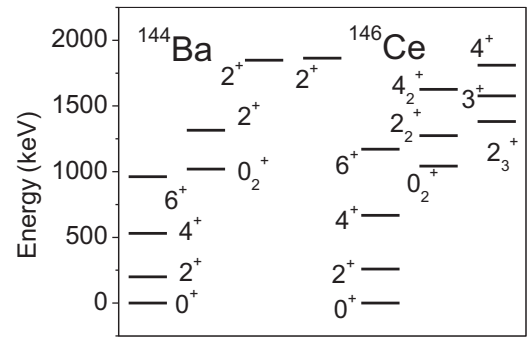

FIG. 4. The partial energy-level spectra of $N = 88$ isotones of Ba and Ce.

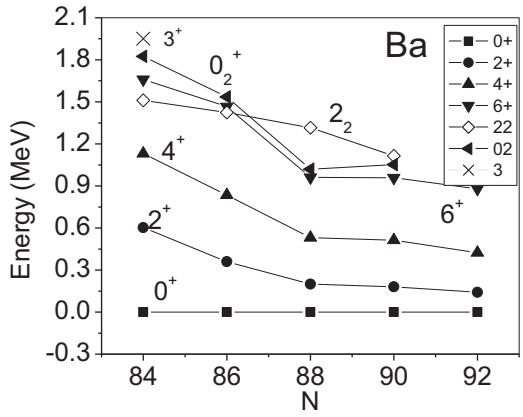

FIG. 5. Energy levels in $^{140-148}$Ba (Ref. [4]).

model [10] to predict the level energies and the $E2$ transition rates and intrinsic structures.

B. Role of N and the $Z = 64$ subshell

As one adds neutron pairs to the closed shell of $N = 82$, the level structure changes profoundly. For example, $E(2_1^+)$ drops by half from 1436 keV in ^{138}Ba to 602 keV in ^{140}Ba. This is a well-known phenomenon, the effect of simultaneous filling of the valence neutrons. Also a regular ground band is formed up to $I^\pi = 12^+$ with $R_{4/2} = 1.877$. At $N = 86$ in ^{142}Ba, $E(2_1^+)$ falls further to 360 keV (Fig. 5) with $R_{4/2} = 2.32$, a value corresponding to an anharmonic vibrator, and the $B(E2, 0_1^+ \rightarrow 2_1^+)$ increases to $0.68\, e^2\, b^2$. The level energy $E(2_1^+)$ at $N = 84$ isotones increases slowly from 602 to 696, 747, and 784 keV for Ba to Gd. In contrast to these, at $N = 86$, the energy $E(2_1^+)$ increases from ∼360 to ∼600 keV with increasing Z (a 60% increase) for Ba to Gd due to $Z = 64$ subshell effects. At $N = 88$, in ^{144}Ba, $E(2_1^+)$ also drops sharply to 199 keV (Fig. 5). But in contrast, at $N = 90$, the drop in $E(2_1^+)$ is only by 18 keV to 181 keV. Again at $N = 92$, $E(2_1^+)$ drops by 40 keV to 142 keV, and the energy ratio $R_{4/2}$ rises to 3.0, the shape transition value [5]. The energy levels of $I^\pi = 4^+, 6^+$ follow the same trend. Thus the slow change at $N = 88$–90 is interesting, which we analyze here in theory. Note the sharp drop in the state $I^\pi = 0_2^+$ (filled triangles in Fig. 5) at $N = 86$–88. Then the nature of $I^\pi = 2_2^+$ (open circle symbol) also changes from $K = 2$ to $K = 0$. The same is true for $N = 90$. The regular yrast bands up to $I^\pi = 12^+$ are formed [4] in the $N \geqslant 84$ Ba isotopes.

III. THEORY

A. The interacting boson model

The interacting boson model IBM is an algebraic model [11] based on the assumption that the collective aspects of low-energy nuclear levels are determined by the valence nucleons (treating the closed shell as an inert core). The correlated nucleon pairs may be represented by $L = 0$, 2 s, and d bosons. As opposed to other boson theories, in IBM one assumes that in the boson-boson interactions, the boson number $N_b = N_p + N_n$ is conserved. This leads to the symmetric group SU(6) with three dynamical subgroup chains of U(5), SU(3), and O(6), which have analytical solutions. The three limiting symmetries correspond to the anharmonic vibrator, the axially deformed rotor and the γ-unstable asymmetric rotor, respectively [11]. Most of the other nuclei may lie on or within the Casten symmetry triangle [13] with the three symmetries at the vertices of the triangle. The path from U(5) to SU(3) is termed [11] as class A, and path U(5) to O(6) is termed as class C. The ^{144,146}Ba isotopes lie on the U(5) to SU(3) path (class A).

The IBM-1 Hamiltonian [11] with four terms (in multipole form),

$$H_{\rm IBM} = \varepsilon n_d + kQQ + k'LL + k''PP \qquad (3)$$

is adequate for the study of relative level energies and $B(E2)$ values. The quadrupole operator $Q^{(2)}$ is given by [11]

$$Q^{(2)} = (s^+d + d^+s)^{(2)} + \chi(d^+d)^{(2)}. \qquad (4)$$

In IBM-2, one counts the proton boson and neutron bosons separately. It has the group structure $SU(6)^\pi \times SU(6)^\nu$ with three dynamic chains as in IBM-1. The IBM-2 Hamiltonian may be defined as in Eq. (5),

$$H_{\rm IBM} = \varepsilon(n_{d\pi} + n_{d\nu}) + \kappa Q_\pi Q_\nu + \lambda M(\xi_1, \xi_2, \xi_3). \qquad (5)$$

Here ε is the single d-boson energy; $n_{d\pi}$ and $n_{d\nu}$ are the number of proton and neutron bosons, respectively. The second and third terms of the Hamiltonian describe the proton-neutron interaction consisting of a quadrupole term and a Majorana-type exchange force term. The coefficients κ and λ represent the strength of these two types of forces. The quadrupole operator is given as follows:

$$Q_\rho(\rho = \pi, \nu) = (d^+s + s^+d)^{(2)} + \chi_{\pi,\nu}(d^+d)^{(2)}. \qquad (6)$$

The parameter $\chi_{\pi,\nu}$ determines the ratio of the two terms.

B. The dynamic pairing plus quadrupole model

It is a submodel of the shell model in which besides the average potential part of the Hamiltonian the residual interactions are limited to the quadrupole interaction, represented by Elliott's SU(3) type separable Q-Q interaction [14]. The nucleon-nucleon interactions in the particle-hole channels are included [10]. This yields the deformed single-particle states and deformed single-particle eigenvalues. Then the monopole pairing in the particle-particle channel is included on equal footing as in the generalized Hartree-Bogoliubov formalism to yield the quasiparticle matrix elements and quasiparticle energies for protons and neutrons. Unlike the ($N < 82$) light Ba isotopes, here the valence particle space in the two oscillator shells of $n = 4,5$ are used for protons and $n = 5,6$ for neutrons, the $Z = 40$, $N = 70$ being the inert core. The inclusion of the upper shell is important since it includes the unique parity subshell, which plays a key role in producing the core deformation.

The pairing plus quadrupole model employs the Hamiltonian [10],

$$H_{\rm PPQ} = H_{\rm sph} + H_{\rm Q} + H_{\rm P}. \qquad (7)$$

TABLE I. The energy levels (keV) in ^{144}Ba compared with theory. The K components (in percentages) from the DPPQM are listed. For $I = 4$ states, the $K = 4$ component is equal to the remainder in 100%. For the DPPQM $X_Q = 75.0$, $F_B = 2.6$. For IBM-1 set 1: $\varepsilon = 720.6$, $k = -44.5$, $k' = -15.45$, $k'' = -17.6$ keV, $\chi = -1.32$. set 2: $\varepsilon = 690.6$, $k = -42.4$, $k' = -13.5$, $k'' = 0.6$ keV, $\chi = -1.32$. In PHINT $QQ = 2k$, ELL $= 2k'$, and PAIR $= k''/2$.

	2_1^+	4_1^+	6_1^+	0_2^+	2_2^+	4_2^+	2_3^+	3_1^+	4_3^+	2_4^+
Expt. [4]	199	530	961.5	1020	1315		1864[a]			
IBM-1 Set 1	208.5	530	944	981	1412	1952	1791	2115	2447	2803
Set 2	200	523	946	1029	1411	1934	1761	2027	2413	2780
IBM-2	196	525	972	1040	1444	1948	1732	1978	2273	2609
DPPQM	251	568	967	828	1164	1471	1483	1774	1944	2062
$K = 0$	99.5	99.3	98.7	100	89.1	94.2	15.3	Zero	11.6	79.2
$K = 2$	0.5	0.7	1.3	Zero	10.9	5.4	84.7	100	85.0	20.8

[a]The $I^\pi = 2^+$, 1848 keV, which decays to 2_1^+, 1^-, and 3^- only, is excluded here.

The first term signifies the average field for the spherical shape, the second term signifies the residual quadrupole interaction between valence nucleons, and the third term signifies the pairing interaction in the BCS formalism. No energy level data are input for $H_{\rm PPQ}$. Only the regional standard parameters are used [10]. The output from $H_{\rm PPQ}$ is used to determine the seven parameters of the Bohr Hamiltonian in Eq. (8), viz. the potential energy $V(\beta,\gamma)$, the three moments of inertia in $T_{\rm rot}$, and the three mass coefficients $B_{\mu\nu}$ in $T_{\rm vib}$ of the vibrational terms. These are used to deduce the static potential-energy surface and the mass coefficients for the kinetic-energy terms of the collective Bohr Hamiltonian $H_{\rm coll}$,

$$H_{\rm coll} = V(\beta,\gamma) + T_{\rm vib}(\beta,\gamma) + T_{\rm rot}(\beta,\gamma). \tag{8}$$

Then the collective Schrödinger equation,

$$H_{\rm coll}\Psi_{\alpha\rm IM} = E_1\Psi_{\alpha\rm IM} \tag{9}$$

is set up and solved numerically in the five-dimensional collective basis, where

$$\Psi_{\alpha\rm IM} = \sum_{K\geqslant 0,\rm even}^{\rm I} A_{\alpha\rm IK}(\beta,\gamma)\phi^{\rm I}_{\rm MK}(\varphi,\vartheta,\psi). \tag{10}$$

The $H_{\rm coll}$ is quantized and solved to yield the collective states energies and wave functions $A_{\alpha IK}(\beta,\gamma)$. The rotational wave function $\phi^{\rm I}_{\rm MK}$ is a symmetrized sum of the standard D functions. The vibrational wave functions $A_{\alpha\rm IK}$ are computed via a numerical solution of the nonlinear integrodifferential equations resulting from the integration of the collective Hamiltonian over the rotational angles (ϕ, ϑ, and ψ).

IV. RESULTS FROM THE IBM AND DPPQM

A. The parameters of the IBM-1 and DPPQM

We have used the computer program PHINT of Scholten [15] for setting the IBM-1 Hamiltonian [Eq. (3)] [11]. The $H_{\rm IBM}$ is set up phenomenologically, based on the boson number $N_{\rm b}$ and the energy-level data. In ^{144}Ba, the energy levels in the ground-state band up to $I^\pi = 10^+$, $E(0_2^+)$, 2_2^+ of 1315 and 1864 keV have been used as input data. The IBM-1 parameters for the two alternative sets are listed in Table I. In ^{146}Ba up to $I^\pi = 8^+$ in the ground-state band and the energies of 0_2^+, 2_2^+, and 2_3^+ are input. For the transition operator, $T(E2)$ is equal to $e_{\rm b}\times Q^{(2)}$. For energies, the coefficient $\chi = -1.32$ is used as applicable for the SU(3) limit [11]. For $B(E2)$ values we used the boson charge $e_{\rm b} = 0.15$ e b and $\chi = -0.80$.

For IBM-2, we have used the computer program NPBOS [16]. The traditional method for fitting the listed parameters was used [17]. In accordance with the standard procedure, one of the parameters was kept fixed at a suitable value, and the others were varied until a best fit was obtained with the available data on experimental low-lying energy levels (up to $I = 10$). The same procedure is repeated for other parameters. The list of IBM-2 parameters is given in Table II. Earlier, the IBM-2 was used in Ref. [18] for the study of $^{140-148}$Ba spectra. Our parameters differ slightly from those of Ref. [18], who have used a smaller value of boson energy ε. However our energy-level fits are as good as of Ref. [18] or better. It may be noted that in the present paper our focus is on the excited $I^\pi = 2^+$ states and their decay characteristics in order to study their nature. In Ref. [18], the 1115-keV $(1,2)^+$ state in ^{146}Ba is not accounted for in the comparison of the IBM-2 spectrum with experiment. For convenience, the parameters used for ^{146}Ba in IBM-2 are also included in Table II.

In the DPPQ model, $H_{\rm sph} = \Sigma_\alpha\varepsilon_\alpha c_\alpha^+ c_\alpha$ with $|\alpha\rangle = |nljm\tau\rangle$ ($\tau = n,p$) as the spherical harmonic-oscillator basis. The spherical single-particle energies ε_α are taken as listed in Ref. [10]. Slight parametrization is allowed in the quadrupole force strength $X = X_Q \times A^{-1.4}$ of H_Q and of the inertial coefficient $F_{\rm B}$ in the collective Bohr Hamiltonian, used to solve for the eigenvalues and the wave functions. The standard value of the quadrupole force strength factor is $X_Q = 70.0$,

TABLE II. The IBM-2 parameters (κ in keV) used in NPBOS. Comparison is made with Subber and Al- Khudair [18] parameters.

Nuclei	ε	κ	χ_ν	χ_π	ξ_2	$\xi_1 = \xi_3$
^{144}Ba	0.77	−0.16	−0.86	−1.50	0.60	0.40
Ref. [18]	0.30	−0.28	−0.4	−0.33	−0.06	0.50
^{146}Ba	0.72	−0.11	−1.0	−1.5	0.1	0.24
Ref. [18]	0.20	−0.27	−0.60	−0.35	−0.19	0.22

and for the inertial renormalization factor $F_B = 2.4$ is used to multiply all the mass coefficients $B_{\mu\nu}$ and the moments of inertia $\theta_k(k = 1$–$3)$. The strength $g_{p,n}$ of the pairing force is kept constant.

Here for ^{144}Ba, X_Q is increased to 75.0 and F_B to 2.6. For ^{146}Ba X_Q is reduced to 71.0 and F_B to 2.6. The quadrupole deformation $\beta = 0.20$ and the $\beta_{RMS} = 0.22$ at $I^\pi = 2_1^+$ with a γ_{RMS} value of 16°. In ^{146}Ba, $\beta = 0.20$ and the $\beta_{RMS} = 0.23$ at $I^\pi = 2_1^+$ with a γ_{RMS} value of 16°. Thus these nuclei are axially symmetric prolate ($\beta > 0$) deformed.

B. Energy spectra and K-band structure

In the DPPQ model, one gets the contribution of the composite K components in any state, which helps to analyze its K admixture. Here in ^{144}Ba, the $K = 0$ components are predicted = 99.5% for the 2_1^+ state, 89.1% for the 2_2 state, and 15.3%, for the 2_3^+ state (Table I). The K-component contribution suggests the 2_2^+ state at 1315 keV as the $K^\pi = 0_2^+$ band state and the 1864-keV 2^+ state as the $K = 2$ state. This is different from the assignments in Ref. [7]. The 1848-keV state seems to be an intruder state here.

The IBM-1 energies for $I^\pi = 8^+, 10^+$ are 1436, 1995 keV (set 1) (or 1454 and 2037 keV for set 2) as compared to 1470, 2044 keV in experiment. The IBM-1 values for other levels are listed in Table I and Fig. 6. Note that a relatively larger value of X_Q in the DPPQM and of the k coefficient of the QQ term in IBM-1 has to be used in ^{144}Ba to produce adequate quadrupole collectivity and low $E(2_1^+)$ as listed in Table I. In IBM-1, the calculated $E(2_3^+)$ is close to the experiment, but in the DPPQM the calculated energy of 2_3^+ is rather low. Higher level energies in the two models differ. These are not known in experiment. Furthermore, in the DPPQ model calculation, the ground band is somewhat condensed, yielding a low $R_{4/2}$ energy ratio. This has been a general feature (limitation) of the model calculation, although other spectral features are well predicted. The spherical single-particle energies are kept constant for the whole region. Also the pairing force strength is kept constant.

The energy-level spectra of ^{144}Ba calculated in IBM-2 are compared with experiment in Fig. 6 for spin I up to 6^+. The fit to ground-state band levels is good. Fair agreement is also

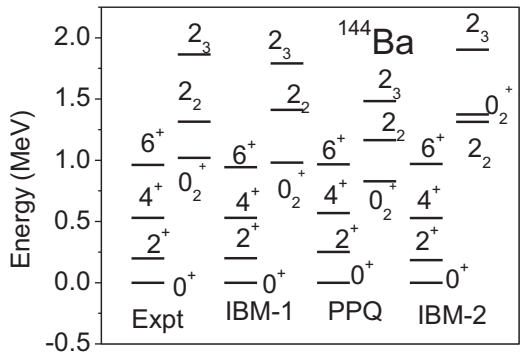

FIG. 6. Energy-level spectra of ^{144}Ba compared with IBM-1 (set 1), the DPPQ model, and IBM-2.

obtained for the excited 2^+ states. But the 0_2^+ state in ^{144}Ba lies high. Our IBM-2 fits are as good as or better than in Ref. [18].

C. $B(E2)$ values and $B(E2)$ ratios in ^{144}Ba

In ^{144}Ba, no $E2$ transition from 2_2^+ to 0_g is observed [4]. This is in consonance with its $K = 0$ character, which predicts weak $E2$ transition to 0_g. The DPPQM small value of $B(E2, 2_2^+ \to 0_1^+) = 0.001e^2\,b^2$ also supports this (Table III). The $B(E2, 2_2^+ \to 4_1^+)$ value in IBM-1 varies fast with a slight change in H_{IBM} parameters so that the ratio $B(E2, 2_2^+ \to 2_1^+/4_1^+)$ varies by a large factor with a slight change in input parameters (see Table III). The DPPQM values agree with experiment within a factor of (2 to 3). Thus for the 1315-keV $I^\pi = 2_2^+$ state, the predictions of theory are reasonable. The IBM-2 predictions of $B(E2)$ ratios are also consistent with experiment.

The larger $K = 2$ component in the 1864-keV 2_3^+ state (Table I) indicates it to be a part of the γ band. For the interband transitions from the 2_3^+ state, the IBM-1 values are not so sensitive to slight variations in input parameters, and theory values agree with experiment, much reduced from the Alaga *et al.* value [21]. Same is true for the DPPQM values. This is expected for a $K = 2\gamma$-vibrational state. There is need for more extensive data for determining the band structure here. The IBM-2 values also vary fast with a slight change in the input parameters. The illustrated values are reasonable. The interband $B(E2, 0_2^+ \to 2_1^+)$ value is smaller than the intraband $B(E2, 0_1^+ \to 2_1)$ value by a factor of 5–10 as given in theory. The $B(E2, 4_1^+ \to 2_1^+)/B(E2, 2_1^+ \to 0_1^+)$ ratio R reduces from 2.0 for a U(5) nucleus to ∼1.5 for SU(3). Here, it is reduced to ∼1.3 (2)! Using the $T_{1/2}$ data in the National Nuclear Data Center (NNDC) [4], the ratio R is indicated to be 1.64 (16). The difference arises on account of the higher value of mean lifetime of 74 ps in Ref. [20] as compared to 49 ps listed in the NNDC [4] for the $4_1^+ \to 2_1^+$ transition. The calculated $B(E2)$ values have been normalized to $B(E2, 2_1^+ \to 0_1^+) = 0.21$ in experiment.

D. Band structure of ^{146}Ba

In IBM-1 we get a good fit to the ground-state band energies (Table IV, Fig. 7). The IBM-1 0_2^+ is low (in set 2), but the higher states of $I^\pi = 2^+$ do have a correspondence to the data. An increase in k'', the coefficient of the pairing term, can raise the 0_2^+ state but affects the level structure adversely (set 1). In IBM-2 (Fig. 7), the ground-state band agrees well with experiment. The states $I^\pi = 2^+$ also are well predicted. In the DPPQ model, again the ground band is condensed, and 2^+ states are higher.

The $N = 86$–88 transition is sharp, but the $N = 88$–90 transition is not as sharp in Ba (Fig. 5) as for higher Z values being maximum for Gd isotopes. This is also reflected in the larger increase in the $B(E2, 2_1^+ \to 0_1^+)$ value at $N = 86$–88 (0.13–$0.21\,e^2\,b^2$ and to $0.27\,e^2\,b^2$ at $N = 90$). The same is well reproduced in the DPPQM and IBM (Table V). No $E2$ operator charge e_p adjustment is performed in the DPPQM calculation here.

TABLE III. $B(E2)$ values (e^2 b^2) and $B(E2)$ ratios in ^{144}Ba compared with DPPQM and IBM values. $e_b = 0.15$, $\chi = -0.8$ for IBM-1. For IBM-2, $e_\pi = 0.06$, $e_\nu = 0.18$. In the DPPQM, a constant charge $e_n = 0.7$ ($e_p = 1 + e_n$) is used.

Transition	Expt. [4,19]	IBM set 1	IBM-1 set 2	DPPQ	Alaga *et al.* [21]	IBM-2
$Q(2^+)$ *e* b	−0.93, 3	−0.93	−0.93	−1.08		−0.904
$B(E2, 2_1^+ \rightarrow 0_1^+)$	0.21, 2	0.21	0.21	0.21		0.21
$B(E2, 4_1^+ \rightarrow 2_1^+)$	0.27, 2[a]	0.30	0.30	0.37		0.263
$B(E2, 2_2^+ \rightarrow 0_1^+/2_1^+)$	0–0.15[b]	0.188	0.198	0.028	0.7	0.137
1315 keV $2_1^+/4_1^+$	1.56, 60	6.3	14	0.48	0.55	1.28
$B(E2, 2_3^+ \rightarrow 0_1^+/2_1^+)$	0.24, 5	0.43	0.51	0.38	0.7	0.56
1864 keV $2_1^+/4_1^+$	4.3, 16	1.95	1.24	2.97	20	0.56
$0_1^+/4_1^+$	1.03, 40	0.84	0.72	1.13	14	0.31
$B(E2, 0_2^+ \rightarrow 2_1^+)$		0.066	0.053	0.231		0.053
$B(E2, 2_2^+ \rightarrow 0_1^+)$	Zero	0.007	0.009	0.001		0.002
$B(E2, 2_2^+ \rightarrow 2_1^+)$		0.038	0.044	0.039		0.013
$B(E2, 2_2^+ \rightarrow 4_1^+)$		0.006	0.003	0.071		0.010
$B(E2, 2_3^+ \rightarrow 0_1^+)$		0.011	0.009	0.010		0.003
$B(E2, 2_3^+ \rightarrow 2_1^+)$		0.025	0.017	0.027		0.005
$B(E2, 2_3^+ \rightarrow 4_1^+)$		0.012	0.014	0.009		0.008

[a]Reference [20].
[b]No 2_2^+-0_{gs} transition is observed. The above value is from an estimate of maximum intensity (Scott *et al.* [8]).

The K-band structure in ^{146}Ba from the DPPQM [10] predicts a pure K state for the ground-state band (Table IV) and a 30% $K = 2$ admixture in the $I^\pi = 2_2^+$ state with a complementary structure for the $I^\pi = 2_3^+$ state. As compared to the $N = 88$ isotope, this is a slightly larger value, in opposition to a more collective structure expected for the $N = 90$ nucleus. But the proximity of the 2_2 to the 2_3 state supports their mixing (also a larger X_Q value in the DPPQM for ^{144}Ba may give rise to this anomaly). In IBM-1 also a larger value of k, the coefficient of the QQ term, is used in ^{144}Ba. The fourth $I^\pi = 2_4^+$ 1566-keV state also has a predominant $K = 2$ component.

The experimental data of the vibrational levels are too scanty to indicate a rotational K-band formation in ^{146}Ba. As stated above, the second $I = 2$ state at 1115 keV is quite close to the 1053-keV 0_2^+ state. However, the phenomenological fit of the IBM and the microscopic DPPQM yield a fair spread of $I = 2$ states (Table IV and Fig. 7).

If our association of the $I = 2$ states from theory with 1115, 1256, and 1566 keV are valid, then we can examine whether the predicted $B(E2)$'s support our band assignments. The absolute values for $E2$ transitions from the vibrational 2^+ states are quite small in both models (Table V). A slight variation in the input IBM parameters (especially the k coefficient in the QQ term) changes the $B(E2)$ values [and $B(E2)$ ratios] by large factors. The larger $B(E2, 2_3 \rightarrow 0_1/2_1)$ ratio compared to $B(E2,2_2 \rightarrow 0_1/2_1)$ is given in IBM-1 and IBM-2 as well as in the DPPQM. In Ref. [4] a larger I_γ for $2_3^+ \rightarrow 0_1^+$ as compared to $2_2^+ \rightarrow 0_1^+$ is indicative of the former being a γ-band state, which agrees with our calculated $B(E2)$ ratios in IBM-1, IBM-2, and the DPPQM.

The ratio $R = B(E2, 4_1^+ \rightarrow 2_1^+)/B(E2, 2_1^+ \rightarrow 0_1^+)$ deduced from $T_{1/2}$ data [4] is 1.59 (16). In theory it varies from 1.42 to 1.62. In Sm at $N = 88$–90 it drops from 1.84 (=0.49/0.266) [22] to 1.52 (=1.05/0.69) [23]. In

TABLE IV. The energy levels (keV) in ^{146}Ba compared with theory and the K components. For the DPPQM, $X_Q = 71.0$, $F_B = 2.6$, and $e_n = 0.70$. IBM-1 set 1 $\varepsilon = 529.8$, $k = -22.25$ keV, $k' = 0.05$, $k'' = 65.6$ keV, and $\chi = -1.32$. IBM-1 set 2 $\varepsilon = 440$, $k = -24.3$, $k' = 5.0$, $k'' = 20.2$ keV, and $\chi = -1.32$.

	2_1^+	4_1^+	6_1^+	0_2^+	2_2^+	4_2^+	2_3^+	3_1^+	4_3^+	2_4^+
Expt.	181.0	513.5	958	1053	1115		1256			1566
IBM-1 set 1	177	503	956	993	1029	1477	1471	1389	2019	2160
IBM-1 set 2	169	519	1034	788	1042	1493	1225	1400	1769	1882
Scott *et al.* [8]	144	475	985	1205	1325	1705	1465	1536		
IBM-2	187	506	947	705	1083	1530	1312	1544	1646	1552
DPPQM	203	493	870	955	1301	1657	1485	1672	1893	2274
$K = 0$	99.7	99.4	98.93	100	70.3	75.1	29.6	0.0	25.4	62.3
$K = 2$	0.3	0.6	1.04		29.7	24.9	70.4	100	74.6	37.7

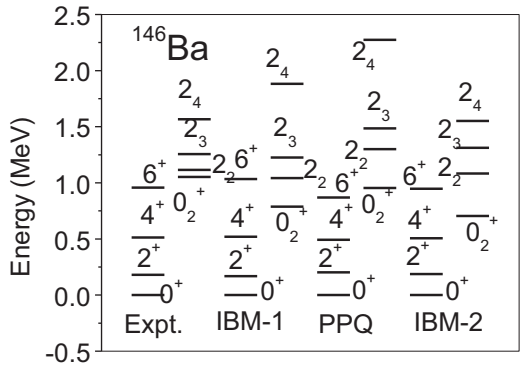

FIG. 7. Energy-level spectra of ^{146}Ba compared with IBM-1 (set 2), the DPPQM, and IBM-2.

^{148,150}Nd, it is almost the same, being 1.54(7) (=0.43/0.28) and 1.55(9) (=0.84/0.54) [24].

The $B(E2, 0_2^+ \rightarrow 2_1^+)$ is also a good measure of the band mixing in a nucleus. Here in ^{146}Ba, it is greater than $0.022\, e^2\, b^2$. In theory it is higher. In Sm it drops from 0.22(2) to $0.157\,(16)\, e^2\, b^2$ at $N = 88$–90 [22,23]. The DPPQM value of $0.23\, e^2\, b^2$ for ^{144}Ba drops to 0.18 in ^{146}Ba. For the $E2$ transitions from the excited states, the $B(E2)$ values from theory have been normalized to $B(E2, 2_1^+ \rightarrow 0_1^+)$ of 0.27(2) in Table V.

E. Comparison with neighboring nuclei

Since the values of E_γ, I_γ are available [4], we compare the experimental $B(E2)$ ratios (upper rows) for $E2$ transitions from the 2_2^+ and 2_3^+ states to the ground band in the $N = 88,90$ isotones with the predictions of the DPPQ model [10,25]

TABLE V. The $B(E2)$ values ($e^2\, b^2$) and $B(E2)$ ratios for ^{146}Ba. For IBM-1 $e_b = 0.14$, $\chi = -1.35$. For IBM-2, $e_\pi = 0.06$, $e_\nu = 0.18$.

Item	Expt. [21,4]	IBM-1 set 1	IBM-1 set 2	DPPQM	IBM-2
$Q(2_1^+)$ $e\,b$	−1.05, 3	−1.07	−1.09	−1.16	−1.11
$B(E2, 2_1^+ \rightarrow 0_1^+)$	0.27, 2	0.27	0.27	0.27	0.27
$B(E2, 4_1^{++} \rightarrow 2_1^+)$	0.39, 4[a]	0.39	0.38	0.44	0.40
$B(E2, 2_2^+ \rightarrow 0_1^+/2_1^+)$	0.32, 5	0.16	0.17	0.027	0.037
1115 keV $\rightarrow 2_1^+/4_1^+$		160	15	1.15	0.73
$B(E2, 2_3^+ \rightarrow 0_1^+/2_1^+)$	0.79, 20	33	1.4	1.04	1.5
1256 keV $\rightarrow 2_1^+/4_1^+$		0 003	0.35	0.46	0.715
$B(E2, 2_4^+ \rightarrow 0_1^+/2_1^+)$	0.63, 9	0.1	0.22	1.1	1.11
1566 keV $\rightarrow 2_1^+/4_1^+$	0.75, 10	2	6	0.26	1.18
$B(E2, 0_2^+ \rightarrow 2_1^+)$	>0.022[a]	0.063	0.040	0.180	0.128
$B(E2, 2_2^+ \rightarrow 0_1^+)$		0.009	0.0061	0.0013	0.0007
$B(E2, 2_2^+ \rightarrow 2_1^+)$		0.057	0.037	0.048	0.020
$B(E2, 2_2^+ \rightarrow 4_1^+)$		0.0004	0.0024	0.042	0.028
$B(E2, 2_3^+ \rightarrow 0_1^+)$		0.0029	0.0075	0.013	0.010
$B(E2, 2_3^+ \rightarrow 2_1^+)$		0.0001	0.005	0.012	0.006
$B(E2, 2_3^+ \rightarrow 4_1^+)$		0.026	0.015	0.025	0.006
$B(E2, 2_4^+ \rightarrow 0_1^+)$		0.0001	0.0003	0.0002	0.0053
$B(E2, 2_4^+ \rightarrow 2_1^+)$		0.0007	0.0011	0.0002	0.0045
$B(E2, 2_4^+ \rightarrow 4_1^+)$		0.0004	0.0002	0.0007	0.0042

[a]Deduced from lifetime data [4].

(Table VI). The Alaga *et al.* value for $B(E2, 2_{exc} \rightarrow 0/2)$ is 0.7 and for $B(E2, 2_{exc} \rightarrow 2/4)$ is 0.55 for $K = 0$ and 20 for $K = 2$. Thus the experimental values for the 2_2^+ and 2_3^+ states vary according to the degree of K admixture in them, which varies with N and Z. Although there is evidence for the 2_2^+ state to be predominantly $K = 0$ and 2_3^+ as $K = 2$, the variation with N and Z is rather complex on account of the $Z = 64$ subshell effects. The DPPQ model values differ from experiment in some cases, but the overall trends are given well.

F. The static characteristics

In the DPPQM, the potential-energy function of the nucleus is given by [10]

$$V(\beta,\gamma) = \Sigma_{i\tau} v_i^2 \eta_i - \Sigma_\tau g_\tau^{-1} \Delta_\tau^2 + (1/2)\chi^{-1}\beta^2. \qquad (11)$$

Here i represents all the deformed quasiparticle (dqp) states of the two oscillator shells, v_i^2 are the occupation probability of a dqp state, η_i is the dqp energy, g_τ is the pairing strength ($\tau = n, p$), and Δ_τ is the calculated pairing gap.

The calculated potential energy $V(\beta, \gamma = 0^\circ)$ for ^{146}Ba is illustrated in Fig. 8. The potential minimum lies on the prolate side at $\beta = 0.20$ with a depth of 1.5 MeV along with the shallow oblate minimum at $\beta = 0.08$ and a depth of 0.2 MeV. The zero-point energy level, indicated by the horizontal line, is just below the spherical barrier and extends from $\beta = 0.14$–0.33. The β_{RMS} is 0.23 and $\gamma_{RMS} = 15.8^\circ$. Thus the nucleus is quite soft to fluctuations in the β variable. This is in consonance with the low-lying 0_2^+ state along with the 2_2^+ state. A similar plot is obtained for ^{144}Ba as well (not shown). The $\beta_{min} = +0.205$, but the prolate depth is $V_d = 0.83$ MeV only (less than for ^{146}Ba) and almost no oblate minimum. Also the zero-point energy level lies at 0.83 MeV above the spherical barrier. The quadrupole moment $Q(2_1^+) = -1.08\, e\, b$ for ^{144}Ba and $-1.16\, e\, b$ for ^{146}Ba almost the same for both isotopes.

G. Occupation numbers of protons and neutrons in Nilsson orbits

It is useful to look at the occupation numbers of protons in deformed Nilsson single-particle orbits, which gives a microscopic view of the effect of filling of protons and neutrons

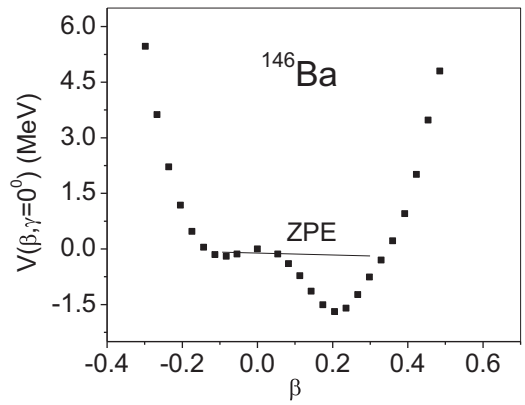

FIG. 8. The static potential-energy curve $V(\beta, \gamma = 0^\circ)$ for ^{146}Ba from the DPPQ model. The horizontal line labeled 'ZPE' denotes zero point energy.

TABLE VI. The $B(E2)$ ratios for $E2$ transitions from $I = 2$ states. Upper rows are for experiment, lower rows are for the DPPQ model values.

$B(E2)$ ratio	^{144}Ba	^{146}Ce	^{148}Nd	$B(E2)$ ratio	^{144}Ba	^{146}Ce	^{148}Nd
2_2-0/2		0.12(4)	0.037(6)	2_2-2/4	1.56(60)		0.9 (5)
DPPQM	0.028	0.04	0.07	DPPQM	0.48	0.71	1.12
2_3-0/2	0.24(5)	1.4(2)	0.57(7)	2_3-2/4	4.3(16)	0.07(3)	0.35(23)
DPPQM	0.38	0.48	0.61	DPPQM	2.97	1.17	0.41
$B(E2)$ ratio	^{146}Ba	^{148}Ce	^{150}Nd	$B(E2)$ ratio	^{146}Ba	^{148}Ce	^{150}Nd
2_2-0/2	0.32(5)	0.012(1)	0.070(35)	2_2-2/4		0.71(11)	0.51(5)
DPPQM	0.027	0.004	0.002	DPPQM	1.15	0.79	0.50
2_3-0/2	0.79(20)	0.76(8)	0.55(11)	2_3-2/4		1.16(14)	3.3(27)
DPPQM	1.1	0.77	0.76	DPPQM	0.26	1.20	2.82

in producing the quadrupole deformation of the nucleus. In the axially symmetric modified oscillator deformed shell model of Nilsson, the single-particle energies are a function of the quadrupole deformation β ($\gamma = 0^\circ$ assumed). Each single-particle subshell is split into $(2j + 1)$ orbits with projection Ω varying from $\frac{1}{2}$ to $(2j + 1)$ in the energy ordering of 1/2, 3/2, 5/2, etc., on the prolate side ($\beta > 0$). Their slopes vary from downward to horizontal and upward progressively.

In the absence of a pairing interaction, these single-particle Nilsson orbits fill according to the Pauli exclusion principle. For example, the proton πg_{72} subshell would fill up to eight protons. The subshell $\pi d_{5/2}$ would fill up to six protons. Thus for Ba isotopes, the six valence protons would occupy the $g_{7/2}$ subshell. However, the energy gap at $\beta = 0$ for $\pi g_{7/2}$ and $\pi d_{5/2}$ being small, the energy ordering for protons would change, and the six protons would be shared between the two subshells. In the presence of the monopole pairing interaction, the occupation probabilities of the single particle would further change due to time-reversed nucleon pair scattering so that the six protons would be shared among the πg_{72}, $\pi d_{5/2}$, and the intruder $\pi h_{11/2}$ subshells.

The valence neutrons would also fill in the neutron single-particle orbits of $\nu f_{7/2}$, $\nu h_{9/2}$, and $\nu i_{13/2}$ subshells in a similar way. Furthermore, the filling of protons and neutrons affect each other. Federman and Pittel [26] noted that in the presence of the spin-orbit partnership coupling of ($l = 5$) $\pi h_{11/2}$ and $\nu h_{9/2}$ subshells, this effect would be enhanced, shifting protons to the $\pi h_{11/2}$ orbitals, causing the increased deformation. In Sm and Gd, at $N = 88$–90 this gives rise to the phenomenon of disappearance of the $Z = 64$ subshell effects at $N = 90$, and a shape phase transition at $N = 88$–90 is exhibited.

Only (relevant) partial data from the previous work [25] on $N = 88$–90 isotones are given in Table VII for $N = 88$ Ba, Ce, Nd and $N = 90$ ^{146}Ba. The data show that, the occupation of the $\pi h_{11/2}$ orbit by the six protons of Ba is rather very small ($\sim$1 proton). So that the spin-orbit partnership effect, called the Federman-Pittel mechanism [26], is not very effective in Ba. Hence the $Z = 64$ subshell effect is not applicable here. This explains the different behavior of E_2 and $B(E2)$ in Ba at $N = 88$–90, different from the $Z = 64$ effects in Nd, Sm, and Gd as discussed above.

TABLE VII. The occupation numbers for protons in ^{144}Ba from the DPPQM, compared with $N = 88$ Ce and Nd and with ^{146}Ba.

	^{144}Ba	^{146}Ce	^{148}Nd	^{146}Ba
$\pi g_{7/2}$	2.508	3.109	3.65	2.512
$\pi d_{5/2}$	1.536	1.915	2.27	1.537
$\pi h_{11/2}$	1.316	2.082	2.95	1.309
Sum	5.360	7.106	8.87	5.358

V. SUMMARY AND DISUSSION

^{144,146}Ba isotopes, with only six protons, do not display well-developed collective rotational K-band structures, except for the ground-state band. In the phenomenological IBM-1 with input energy levels, it is possible to fit the ground-state band level energies very well, but for the vibrational bands, the predictions are not so close. The predictions from the dynamic PPQ model are slightly better for the $B(E2)$ values than in IBM-1 and IBM-2, but the energy scale deviates from the experiment.

The $I^\pi = 2^+$ 1848-keV state in ^{144}Ba seems to be an intruder for the IBM. On the basis of predicted K-component structures we have assigned the 2_2^+ and 2_3^+ states to the $K = 0$ and $K = 2$ bands, respectively. In ^{144}Ba the interband $B(E2)$ ratios are well predicted. In ^{146}Ba, the few data are fairly reproduced. In ^{146}Ba, we have assigned 1115 and 1256 keV to $I^\pi = 2^+$ and $K = 0$ and 2, respectively. The prediction of the very weak $E2$ transition varies by a large factor by slight variation in $H_{\rm IBM}$ parameters and the χ coefficient of the (d^+d) term in the $T(E2)$ operator. The occupation numbers of protons in the $\pi g_{7/2}$, $\pi d_{5/2}$, and $\pi h_{11/2}$ Nilsson orbits in Ba at $N = 88$ and $N = 90$ calculated in the pairing part of the DPPQM remain the same, viz. about 2.5, 1.5, and 1.3, respectively. The low proton occupancy in the $\pi h_{11/2}$ orbit enables little scope for the spin-orbit partnership of $\nu h_{9/2}$ and $\pi h_{11/2}$ as applicable to higher Z isotones, which explains their special behavior at $N = 88$–90.

ACKNOWLEDGMENTS

The postretirement association with Ramjas College, University of Delhi, is gratefully acknowledged by J.B.G. M.S. thanks the Principal of Hindu College for encouragement.

[1] B. R. Mottelson and S. G. Nilsson, Phys. Rev. **99**, 1615 (1955).
[2] R. F. Casten, D. D. Warner, D. S. Brenner, and R. L. Gill, Phys. Rev. Lett. **47**, 1433 (1981).
[3] R. F. Casten and N. V. Zamfir, J. Phys. G: Nucl. Part. Phys. **22**, 1521 (1996).
[4] Brookhaven National Laboratory, Chart of nuclides of National Nuclear Data Center, http://www.nndc.bnl.gov/ENSDF/
[5] F. Iachello, Phys. Rev. Lett. **87**, 052502 (2001).
[6] L. K. Peker and J. K. Tuli, Nucl. Data Sheets **82**, 187 (1997).
[7] M. Sakai, At. Data Nucl. Data Tables **31**, 399 (1984).
[8] S. M. Scott, W. D. Hamilton, P. Hungerford, D. D. Warner, G. Jung, K. D. Wunsch, and B. Pfeiffer, J. Phys. G: Nucl. Part. Phys. **6**, 1291 (1990).
[9] K. Kumar and J. B. Gupta, Nucl. Phys. A **694**, 199 (2001).
[10] K. Kumar and M. Baranger, Nucl. Phys. A **110**, 529 (1968).
[11] F. Iachello and A. Arima, *The Interacting Boson Model* (Cambridge University Press, Cambridge, UK, 1987).
[12] J. B. Gupta, Int. J. Mod. Phys. E **22**, 1350023 (2013).
[13] R. F. Casten, *Nuclear Structure from a Simple Perspective* (Oxford University Press, New York, 1990).
[14] J. P. Elliott, Proc. R. Soc. London, Ser. A **245**, 128 (1958).
[15] O. Scholten, *Computer program package* PHINT.
[16] T. Otsuka, *Computer Program NPBOS*, University of Tokyo, Japan (1987).
[17] K. Heyde, J. Moreau, and M. Waroquier, Phys. Rev. C **29**, 1859 (1984).
[18] A. R. H. Subber and F. H. Al-Khudair, Phys. Scr. **84**, 035201 (2011).
[19] S. Raman, C. W. Nestor, and P. Tikkanen, At. Data Nucl. Data Tables **78**, 1 (2001).
[20] T. M. Shneidman, R. V. Jolos; R. Krucken, A. Aprahamian, D. Cline, J. R. Cooper, M. Cromaz, R. M. Clark, C. Hutter, A. O. Macchiavelli, W. Scheid, M. A. Stoyer, and C. Y. Wu, Eur. Phys. J. A **25**, 387 (2005).
[21] G. Alaga, K. Alder, A. Bohr, and B. R. Mottelson, Mat.-Fys. Medd.-K. Dan. Vidensk. Selsk. **29**, 9 (1955).
[22] H. G. Börner, P. Mutti, M. Jentschel, N. V. Zamfir, R. F. Casten, E. A. McCutchan, and R. Krücken, Phys. Rev. C **73**, 034314 (2006).
[23] R. F. Casten, M. Wilhelm, E. Radermacher, N. V. Zamfir, and P. von Brentano, Phys. Rev. C **57**, R1553 (1998).
[24] C. Fahlander, A. Backlin, L. Hasselgren, C. Pomar, G. Fossnert, and J. E. Thun, Inst. Phys. Conf. Ser. **49**, 291 (1980).
[25] J. B. Gupta, Phys. Rev. C **87**, 064318 (2013).
[26] P. Federman and S. Pittel, Phys. Lett. B **77**, 29 (1978).